Neuronal spiking activity highlights a gradient of epileptogenicity in human tuberous sclerosis lesions

Elodie Despouy, Jonathan Curot, Marie Denuelle, Martin Deudon, Jean-Christophe Sol, Jean-Albert Lotterie, Leila Reddy, Lionel G Nowak, Jérémie Pariente, Simon Thorpe, et al.

Clinical Neurophysiology 130 (2019) 537–547

Contents lists available at ScienceDirect

Clinical Neurophysiology

journal homepage: www.elsevier.com/locate/clinph

Neuronal spiking activity highlights a gradient of epileptogenicity in human tuberous sclerosis lesions

Elodie Despouy [a,b,c,*,1], Jonathan Curot [a,b,d,1], Marie Denuelle [d], Martin Deudon [a,b], Jean-Christophe Sol [e,f], Jean-Albert Lotterie [e,g], Leila Reddy [a,b], Lionel G. Nowak [a,b], Jérémie Pariente [e,h], Simon J. Thorpe [a,b], Luc Valton [a,b,d], Emmanuel J. Barbeau [a,b]

[a] Centre de Recherche Cerveau et Cognition, Université de Toulouse, Université Paul Sabatier Toulouse, Toulouse F-31330, France
[b] Centre National de la Recherche Scientifique, CerCo, UMR 5549, Toulouse F-31052, France
[c] DIXI Medical, Chaudefontaine F-25640, France
[d] Explorations Neurophysiologiques, Hôpital Purpan, Université de Toulouse, Toulouse F-31300, France
[e] INSERM, U1214, TONIC, Toulouse Mind and Brain Institute, Toulouse F-31052, France
[f] Neurochirurgie, Hôpital Purpan, Université de Toulouse, Toulouse F-31300, France
[g] Radiochirurgie stéréotaxique, Hôpital Purpan, Université de Toulouse, Toulouse F-31300, France
[h] Neurologie, Hôpital Purpan, Université de Toulouse, Toulouse F-31300, France

ARTICLE INFO

Article history:
Accepted 25 December 2018
Available online 30 January 2019

Keywords:
Stereoelectroencephalography (SEEG)
Microelectrode
Tuberous sclerosis complex
Epilepsy
Action potentials

HIGHLIGHTS

- First recordings of spiking neuronal activity in the tuber and perituberal tissue using new hybrid electrodes equipped with tetrodes.
- Gradient of epileptogenicity running from the tuber to perituberal tissue revealed by multi-scale analyses.
- Observation of interactions both within and between the tuber and peritubér.

ABSTRACT

Objective: The mechanisms underlying epileptogenicity in tuberous sclerosis complex (TSC) are poorly understood.
Methods: We analysed neuronal spiking activity (84 neurons), fast ripples (FRs), local field potentials and intracranial electroencephalogram during interictal epileptiform discharges (IEDs) in the tuber and peritubér of a patient using novel hybrid electrodes equipped with tetrodes.
Results: IEDs were recorded in the tuber and peritubér. FRs were recorded only in the tuber and only with the microelectrodes. A larger proportion of neurons in the tuber (57%) than in the peritubér (17%) had firing-rates modulated around IEDs.
Conclusions: A multi-scale analysis of neuronal activity, FRs and IEDs indicates a gradient of epileptogenicity running from the tuber to the peritubér.
Significance: We demonstrate, for the first time *in vivo*, a gradient of epileptogenicity from the tuber to the peritubér, which paves the way for future models of epilepsy in TSC. Our results also question the extent of the neurosurgical resection, including or not the peritubér, that needs to be made in these patients.

1. Introduction

About 90% of patients with tuberous sclerosis complex (TSC) develop epilepsy (Chu-Shore et al., 2009). Around 50–80% of these are pharmacoresistant, such that resection of the tuber from which the seizures originate must be considered in some patients (Kahane and Landré, 2008; Bartolomei et al., 2017). Tuber

Abbreviations: ADC, apparent diffusion coefficient; EEG, electroencephalography; EI, epileptogenicity index; FLAIR, fluid-attenuated inversion recovery; FRs, fast ripples; HFOs, high-frequency oscillations; IED, interictal epileptiform discharge; iEEG, intracranial electroencephalography; LFP, local field potential; SEEG, stereoelectroencephalography; SOZ, seizure onset zone; TSC, tuberous sclerosis complex.

* Corresponding author at: CerCo CNRS, UMR 5549, Université Toulouse III, CHU Purpan, Pavillon Baudot, BP 25202, 31052 Toulouse Cedex, France.
E-mail address: elodie.despouy@cnrs.fr (E. Despouy).
[1] These authors contributed equally to this work.

https://doi.org/10.1016/j.clinph.2018.12.013
1388-2457/

delineation and surgical decision are, however, complex processes. Most patients have multiple tubers, but not all are associated with electroencephalography (EEG) abnormalities. Multiple independent epileptic foci can sometimes be found. In other instances, some tubers are associated with interictal pathological activities, but do not belong to the seizure onset zone (SOZ). Progress must therefore be made about our understanding of the SOZ in TSC to inform neurosurgery.

Even if an isolated tuber is suspected of being related to the SOZ, delineating the exact borders of the epileptogenic tissue is often difficult. In addition, the tuber is surrounded by perituberal tissue that can also be pathological. The exact role of the tuber and perituberal tissue in seizures remains unclear. For example, the high-frequency oscillations (HFOs), and more particularly the fast ripples (FRs) between 200 and 600 Hz, that are regarded as biomarkers of SOZs, are not always found in TSC (Mohamed et al., 2012; Okanishi et al., 2014; Ferrari-Marinho et al., 2015; Kannan et al., 2016). Furthermore, although several studies have reported that seizures arise from tubers, or even from tuber centres, before propagating to a *tuber rim*, resection of tubers fails to control seizures in more than 40% of patients (Jansen et al., 2007; Jacobs et al., 2008; Ma et al., 2012; Mohamed et al., 2012; Kannan et al., 2016). Resection beyond the tuber's apparent limits is associated with a greater probability of seizure relief (Fallah et al., 2015). It has therefore been suggested that although perituberal tissue appears normal on conventional MRI, it may also be epileptogenic, and seizures may also originate from there (Madhavan et al., 2007; Sosunov et al., 2008; Major et al., 2009; Marcotte et al., 2012; Chalifoux et al., 2013; Ruppe et al., 2014). In support of this proposal, 7 T MRI has revealed previously undetected lesions, including microtubers, which are tuber-like spherical microscopic collection of giant cells, dysplastic neurons and astrocytes, with a diameter of about 285 microns (Sosunov et al., 2008, 2015; Chalifoux et al., 2013; Peters et al., 2015). Overall, these recent results suggest a gradient of abnormality running from the tuber to the perituberal tissue (Marcotte et al., 2012; Peters et al., 2015), departing from previous conceptions of TSC that report a discontinuity between the tuber and perituber (Feliciano et al., 2013).

Intracranial EEG (iEEG) studies in TSC have relied thus far on electrocorticography, depth macroelectrode recording, or a combination of the two. This scale is too large, however, to analyse activity at the neuronal level or within microtubers. Only microelectrodes (20–50 μm diameter) can simultaneously record local field potentials (LFPs) on a submillimeter scale along with neuronal activity. These more localised signals could help us understand the dynamics of the epileptogenic interactions between the tuber and perituberal tissue in TSC. Only rare multi-scale analyses, which did not include any patient with TSC, could demonstrate that interictal epileptiform discharges or seizure initiation relied on heterogeneous neuronal firing patterns. This lead to the revision of the historical conception of a paroxysm of hypersynchronous excitatory activity (Truccolo et al., 2011; Lambrecq et al., 2017) but much remains to be clarified in this field. To our knowledge, furthermore, no study has so far used intracranial microelectrodes to explore in vivo the electrophysiological features of tubers and perituberal tissue in humans. Whether epileptic activity during TSC is also related to heterogeneous neuronal firing pattern thus remains to be investigated.

As a consequence, the specific mechanisms behind epileptogenicity in TSC are not fully understood. The purpose of our study was therefore to analyse the interictal activity of the tuber and perituberal tissue on different spatial scales, in order to better understand their respective roles in the genesis of epileptic activity in human TSC. We hypothesised that both are involved in the genesis of epileptic activities, as there is independent evidence in the literature. The roles of the tuber and perituberal tissue may differ, given that they are histologically distinct, but they may also be interdependent. To study this possible interdependence and to overcome spatial limits, we analysed neuronal activity, FRs, iEEG and LFPs during interictal epileptiform discharges (IEDs), using simultaneous macro- and microelectrode recordings with a newly designed electrode equipped with tetrodes.

2. Methods

2.1. Patient

The patient was a 39-year-old woman with TSC. She had developed partial epilepsy at the age of 3 years, which became pharmacoresistant in her childhood. Seizure semiology was stereotyped: vegetative symptoms, smothering sensation, fear, unpleasant taste, and hypersalivation followed by hyperkinetic symptoms (pedalling, trunk swaying, agitation), without any language disorder or memory impairment.

2.2. Procedure

Non-invasive assessments failed to localise the SOZ with certainty. Two scalp video-EEG sessions recorded mostly right temporal IEDs and several clinically stereotyped seizures with rapid or rhythmic theta discharge on bilateral anterior regions, or else a spike-and-wave complex in the right hemisphere before the discharge or bilateral rhythmic theta activity. MRI revealed multiple tubers, but no subependymal giant cell astrocytomas or periventricular nodules. A right insular tuber seemed to differ from the others, as it had greater cortical thickness, more pronounced white and gray matter dedifferentiation and a higher apparent diffusion coefficient (ADC). Interictal FDG-PET revealed focal hypometabolism of all tubers.

Our main hypothesis was that a SOZ was located in the right insula, related to the large insular tuber, with propagation in the anterior cingulate cortex. We could not exclude the possibility of either early involvement of the frontal lobe or a purely frontal SOZ involving the anterior cingulate cortex. Furthermore, we could not precisely delineate the insular extension of the SOZ.

In clinical practice, the SOZ is an electroclinical definition corresponding to the "site of beginning and of the primary organisation of the seizures" among the cerebral regions involved in the seizures (Munari and Bancaud, 1987; Kahane et al., 2006; Bartolomei et al., 2017). To better delineate the SOZ, the patient underwent stereoelectroencephalography (SEEG) (Fig. 1). The antiepileptic treatment (lacosamide and oxcarbazepine) was gradually reduced from the 5th day post-implantation, to facilitate seizure occurrence.

The patient received detailed information about the objectives of the SEEG and the use of hybrid electrodes. She signed an informed consent form for the implantation and for the use of the EEG data for research purposes. Implantation of the hybrid electrodes was approved by the local ethics committee and French Drug and Health Products Safety Agency (CPP Sud-Ouest et Outre-Mer I, no.1-14-23 and ANSM 2014-A00747-40).

2.3. MRI

Preoperative imaging was performed on a 3 T MAGNETOM Skyra MRI scanner (Siemens, Erlangen, Germany). Delimitation of the tuber and perituberal tissue was done visually by a neuroradiologist blind to the electrode implantation and to the purpose of the study. Tuber delimitation criteria were higher ADC, T1-WI hypointensity, T2-WI hyperintensity, fluid-attenuated inversion

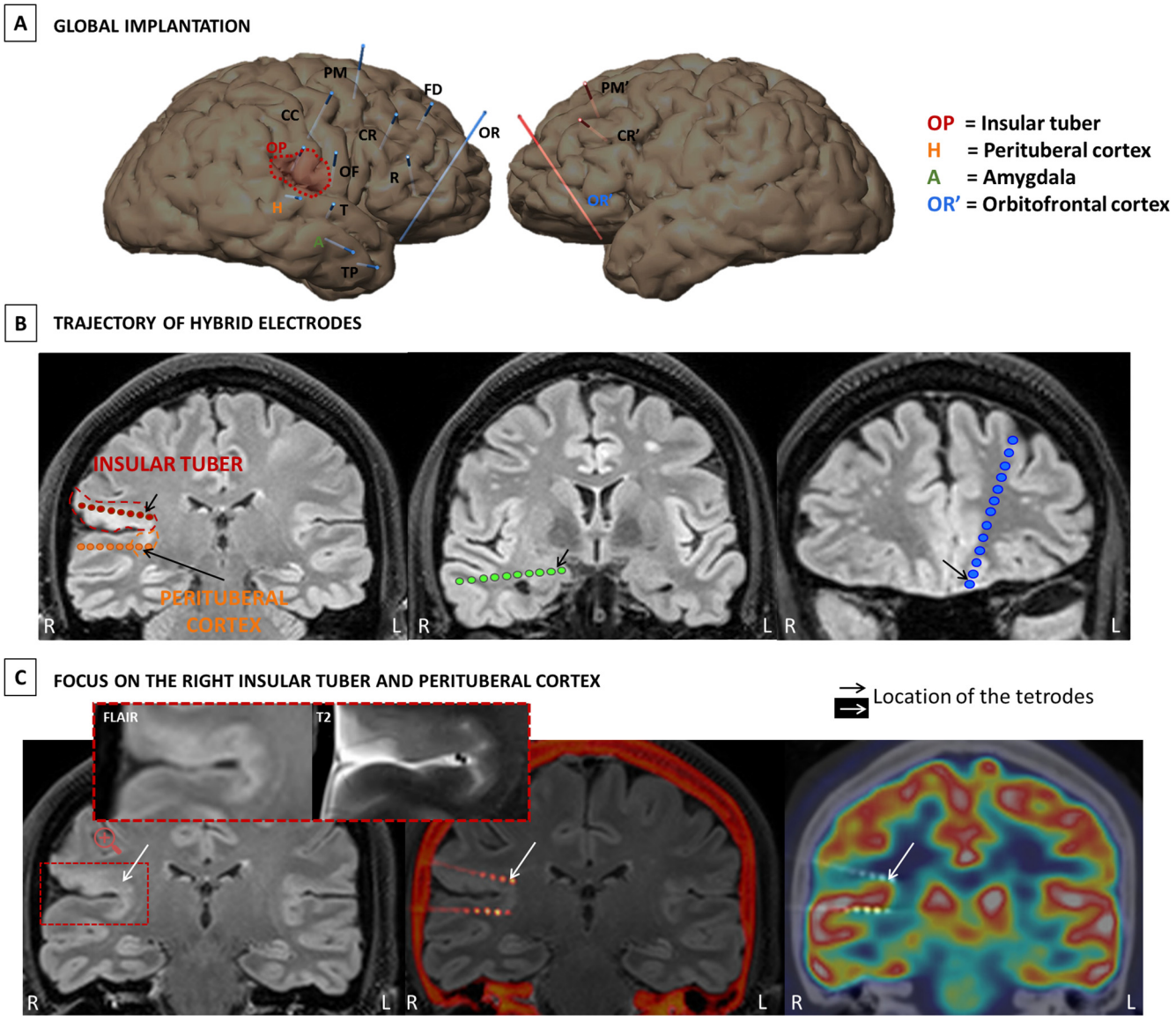

Fig. 1. Tuber and perituber delimitation were based on MRI criteria (see Section 2.3 MRI, (Grajkowska et al., 2010; Kannan et al., 2016)). (A) Complete implantation with location of the four hybrid electrodes (coloured circles) and the 11 clinical macroelectrodes. Each macroelectrode is named by a black letter. Hybrid electrodes are names with a colored letter (H, OP, A and OR′). One hybrid electrode targeted the insular tuber, and one the insular perituberal tissue. The two others targeted cortex that appeared normal on MRI (right amygdala, left orbitofrontal cortex (see B)). Clinical macroelectrode OF was located adjacent to the insular perituber. Clinical macroelectrode PM spanned another tuber located in the medial superior frontal gyrus. (B) T2-FLAIR imaging with a reconstruction showing the location of the hybrid electrodes. One hybrid electrode (red) targeted the right insular tuber suspected of being associated with the SOZ, one (orange) targeted the peritubercal tissue, and the two others targeted apparently healthy cortex: (amygdala (green) and orbitofrontal cortex (blue). The coloured circles are the macrocontacts. The location of the microelectrodes is indicated by the black arrows. (C) Aspect of the right insular tuber and perituberal tissue on MRI. The middle picture is the fusion of CT-scan post-implantation and MRI FLAIR pre-implantation. The picture on the right corresponds to FDG-PET imaging revealing hypometabolism in the tuber.

recovery (FLAIR) areas distinct from the surrounding cortex, loss of gray and white matter differentiation, enlargement of the cortical layer, and no contrast enhancement with gadolinium (Grajkowska et al., 2010). Perituberal tissue was deemed to be the area adjacent to the tuber, but which did not meet the previous criteria and appeared normal on MRI (Kannan et al., 2016).

2.4. Electrodes and recordings

The choice of electrode location was based solely on pre-SEEG clinical observations and on hypotheses about the location of the SOZ based on non-invasive assessment. Eleven semi-rigid multi-lead clinical depth macroelectrodes (nine in the right hemisphere, two in the left; Microdeep, DIXI Medical, France) and four new hybrid electrodes (three right, one left; designed by DIXI Medical) were implanted (Fig. 1). The detail of each electrode placement and type is available in Table 1. Each electrode is identified by letters (e.g. H). An uppercase letter refers to a macroelectrode and the corresponding lowercase letter refers to the tetrodes of that same macroelectrode (e.g. h). Three electrodes (2 hybrids – OP-op and H-h – and 1 macroelectrode – OF) targeted the right insular cortex. One macroelectrode – PM – targeted another small tuber located in the medial prefrontal cortex and can be considered as a potential control electrode.

The macroelectrodes had a diameter of 0.8 mm and contained 5–18 contacts (platinum/iridium) 2 mm long and 1.5 mm apart. The hybrid electrodes each consisted of a clinical macroelectrode (diameter: 0.8 mm) equipped with three tetrodes (four microelec-

Table 1
Details of electrode placement.

Electrode	Hemisphere	Type	Nb of contacts macro/micro	Lateral contact	Medial contact	Additional information
A*	Right	hybrid	6/12	Medial temporal gyrus (BA21)	Amygdala	/
CC	Right	clinical	15	Central gyrus (BA4)	Anterior cingulate (BA24)	/
CR	Right	clinical	15	Medium frontal gyrus (BA9)	Anterior cingulate (BA24)	/
FD	Right	clinical	8	Superior frontal gyrus (BA9)	Superior frontal gyrus (BA9)	/
H*	Right	hybrid	6/12	Superior temporal gyrus (BA42)	Posterior inferior insula	Medial contacts in the insular perituberal cortex
OF	Right	clinical	10	Central operculum (BA4)	Medium superior insula	Medial contacts close to the insular tuber
OP*	Right	hybrid	6/12	Parietal operculum (BA1/2/3/43)	Posterior superior insula	Medial contacts in the insular tuber
OR	Right	clinical	18	Superior frontal gyrus (BA10)	Straight gyrus (BA12)	/
PM	Right	clinical	8	Superior frontal gyrus (BA8)	Superior frontal gyrus (BA8)	Medial contacts span a frontal tuber
R	Right	clinical	15	Inferior temporal gyrus (BA45)	Anterior cingulate (BA24/32)	/
T	Right	clinical	8	Superior temporal gyrus (BA22)	Anterior inferior insula	/
TP	Right	clinical	10	Medial temporal gyrus (BA38)	Superior temporal gyrus (BA 38)	/
CR'	Left	clinical	12	Medium frontal gyrus (BA9/46)	Anterior cingulate (BA24)	/
OR'*	Left	hybrid	6/12	Superior frontal gyrus (BA10)	Straight gyrus (BA12)	/
PM'	Left	clinical	8	Superior frontal gyrus (BA8)	Superior frontal gyrus (BA8)	/

trodes each, details in Fig. 2) that protruded 2 mm from the shaft between the first and second most medial macrocontacts. Tetrodes were extended from the electrode shaft after implantation, using a micrometer screw. These new hybrid electrodes have been under clinical investigation in our epilepsy centre since 2015, with an agreement to implant up to four hybrid electrodes per patient. Computer-assisted matching between post-implantation CT-scan and preimplantation 3D-MRI data allowed us to localize the electrodes' contacts.

Macrocontact signals were recorded using two SystemPLUS EVOLUTION 64-channel acquisition units (Micromed, France) at a sampling rate of 2048 Hz (anti-aliasing filter: 926.7 Hz; high-pass filter: 0.15 Hz; low-pass filter: 1000 Hz). Microelectrode signals were recorded using a 64-channel Cerebus System (Blackrock Microsystems, Salt Lake City, UT, USA) at a sampling rate of 30 kHz (0.3–7.5 kHz bandwidth). Line noise cancellation at 50 Hz was applied. A macrocontact located in the white matter was used as a reference for both systems. Macrocontacts were recorded 24/24 h. Microelectrodes were recorded for 1 hour in five morning sessions on Days 2, 5, 6, 7 and 8, while the patient watched TV show episodes.

We voluntarily focused our analyses on the recordings from the four hybrid electrodes to allow multi-scale comparisons between different areas, of the neuronal activity and the fast ripples notably. The location of the four hybrids covers different types of tissues (tuber, peritube, apparently normal homolateral and contralateral tissue) which was sufficient to test our hypotheses.

2.5. Epileptic event identification

Monopolar montages and reformatted bipolar montages were used for micro- and macroelectrode recordings, respectively. Simultaneous EEG recordings on micro- and macroelectrodes were analysed with a toolbox developed in our laboratory (Micmac). The microsignal was reviewed manually. Noisy periods or channels were excluded.

IEDs were mostly brief (<1 s) or sporadic bursts of intermittent spike-and-wave activity, sometimes followed by gamma or ripple activity (Fig. 3A). IEDs that occurred during the 5 × 1 hours of simultaneous recordings on macro- and microelectrodes were visually identified by two independent experts in EEG analyses (ED, JC) according to traditional morphological characteristics used in clinical practice: sharpness and duration, clearly distinguishable from background activity (Gotman and Gloor, 1976). IEDs were marked independently of FRs.

FRs were analysed during the same 5 × 1 hours of recordings. FRs were sought in the iEEG and LFPs recorded on both the hybrid and clinical macroelectrodes. There were three criteria for identifying FRs: an oscillation visible in both the raw data and the filtered signal (200–600-Hz bandpass finite impulse response filter to reduce ringing); at least four oscillations; and time-frequency analysis resulting in circumscribed areas in the time–frequency plane in the FR band to avoid artefacts and *false ripples* created by filtering (Bénar et al., 2010; Zijlmans et al., 2012). As microelectrode recordings can contain movement artefacts and have higher electromagnetic sensitivity, FRs on the microelectrodes were visually reviewed by two of the authors (ED, JC) during the first 10 min of each hour of recording. The raw and filtered signal (200–600 Hz) of four microwires (i.e. corresponding to a single tetrode) were visualised simultaneously using a 0.6 s time window. Cohen's kappa coefficient (κ) was computed for each channel (Ferrari-Marinho et al., 2015). If $\kappa < 0.6$, both examiners reanalysed the channel. Otherwise, the remaining 50 min were then analysed by one examiner. On the macroelectrodes, FRs were first visually sought by one examiner. To confirm the results, we subsequently used Delphos (an automatic detector which improves the detectability of HFOs by applying a linear whitening (i.e. flattening) transformation to enhance the fast oscillations while preserving an optimal signal to noise ratio) (Roehri et al., 2016).

2.6. Spike sorting

Each microwire signal was bandpass filtered using a Butterworth filter (300–3000 Hz) and whitened. We detected action potentials offline on each separate tetrode. Spike sorting was performed using SpyKING CIRCUS (with a template matching-based algorithm) (Yger et al., 2018). We took into account different quality metrics (interspike interval, scatterplots of the different clus-

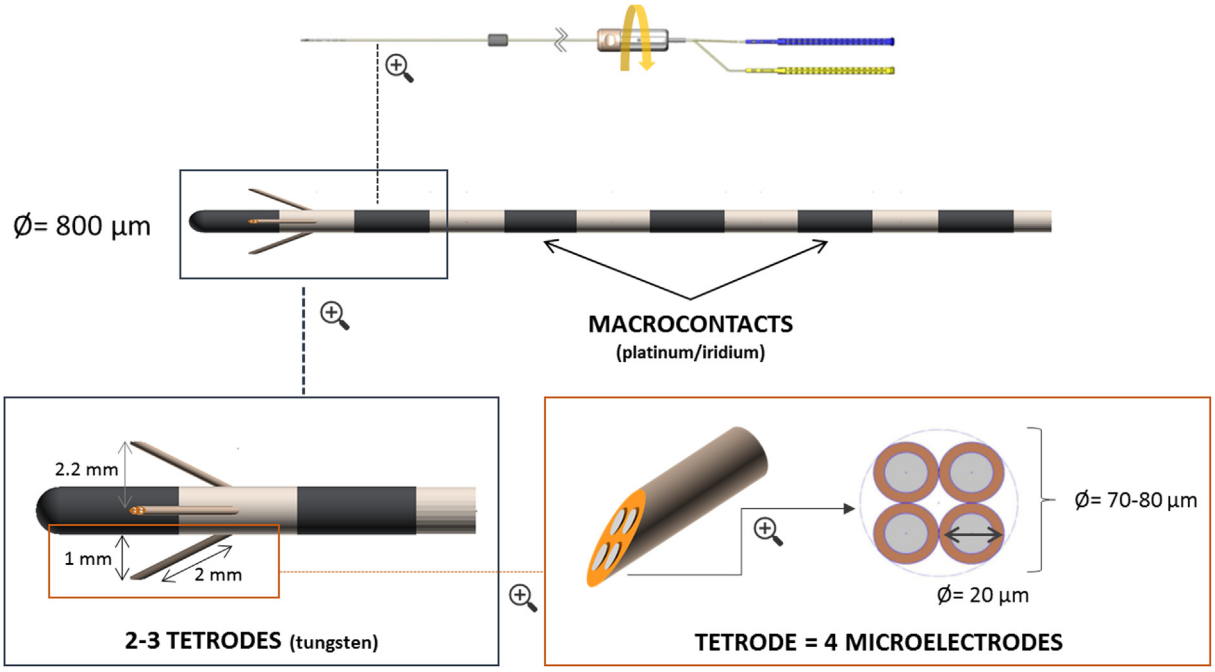

Fig. 2. New hybrid micro-macroelectrode used in this study. The difference with a clinical macroelectrode is the inclusion of three tetrodes that can be extended from the shaft between the most medial macrocontacts by up to 2 mm. Each tetrode is composed of four tungsten microwires with a diameter of 20 µm (overall diameter: 70–80 µm).

ters, amplitude over time, autocorrelogram, crosscorrelogram, refractory period violations; Supplementary Fig. S1) to optimize spike sorting (Hill et al., 2011). An action potential was detected if the amplitude was above a threshold set at six times the median of the absolute deviation of the voltage. The resulting data were inspected manually and refined using the MATLAB graphical interface.

To visualise the patterns of neuronal activity around the IEDs, we constructed peristimulus raster plots and time histograms (bin duration = 10 ms) for a period extending from 1 s before and to 1 s after each event. After visual inspection of the mean LFP of all IEDs, we defined five distinct time periods around the IED peaks (Fig. 4A). We considered that a neuron was modulated around an IED if there was a significant difference in the firing rate in at least one of the four periods of interest we had defined, compared with the baseline. To account for the nonparametric distribution of the action potential firing rate, we calculated a Kruskal-Wallis one-way analysis of variance (ANOVA) to test the equality of medians ($p < 0.05$) for the firing rate in the baseline period and each period of interest (Keller et al., 2010). We then ran Dunn's post hoc test with the Holm-Sidak correction to account for the number of time periods being compared.

Finally, we performed cross-correlation analyses to evaluate the functional interactions between all pairs of neurons that were modulated by IEDs (bin duration: 1 ms, period of analysis: [−80, 80] ms around IEDs) (Amarasingham et al., 2012). We also excluded portions of 2 s of signal around IEDs to investigate basal interactions. These analyses were performed with the Python packages Neo and Elephant (Garcia et al., 2014). To estimate the significance level of the crosscorrelograms for basal interactions, each target spike train was jittered by a random amount (zero-mean Gaussian distribution, $SD = 30$ ms) and the corresponding crosscorrelogram recalculated (Alvarado-Rojas et al., 2013). This procedure was repeated 1000 times and the 99% confidence interval was estimated. For crosscorrelograms computed around the IEDs, we used the shift predictor to correct for the stimulus-induced relationship (Narayanan and Laubach, 2009).

2.7. Connectivity during seizures and IEDs

Direct electrical brain stimulation is a standard clinical procedure for assessing the local propensity of the stimulated brain areas to induce seizures and allow for functional mapping. Bipolar electrical brain stimulation (1 or 50 Hz, 1-ms pulses) was applied between adjacent macrocontacts.

We calculated the epileptogenicity index (EI) using the AnyWave toolbox (Colombet et al., 2015). EI is a mathematical index which characterizes the involvement of a given brain structure in the generation of high-frequency (beta or gamma) iEEG fluctuations, as observed during the transitions between ictal and interictal activity (Bartolomei et al., 2008). The normalised value of EI ranges from 0 (no involvement of brain structure) to 1 (brain structure generates a rapid discharge, time to seizure onset is minimal).

3. Results

Four spontaneous seizures were recorded with the macroelectrodes. None of them occurred during the 5 × 1 hour microelectrode recording periods. We focused our analyses on neuronal activity during IEDs.

3.1. IEDs

IED patterns were highly similar to those recorded at the start of the seizures (Supplementary Fig. S2). IEDs were recorded with both micro- and macroelectrodes (on the macrocontacts immediately adjacent to the microelectrodes) and synchronously involved the insular tuber (OP-op) and perituberal tissue (H-h). They had a higher amplitude in the tuber and some were recorded solely in the tuber (Supplementary Fig. S3). The microelectrodes enabled us to detect additional IEDs in perituberal tissue that were not picked up by the macroelectrodes (Fig. 3A). IEDs that were only recorded on the microelectrodes had lower amplitudes (Supplementary Fig. S3). IEDs were not recorded in any other brain region or tuber (excepted on electrode OF, which was not a hybrid

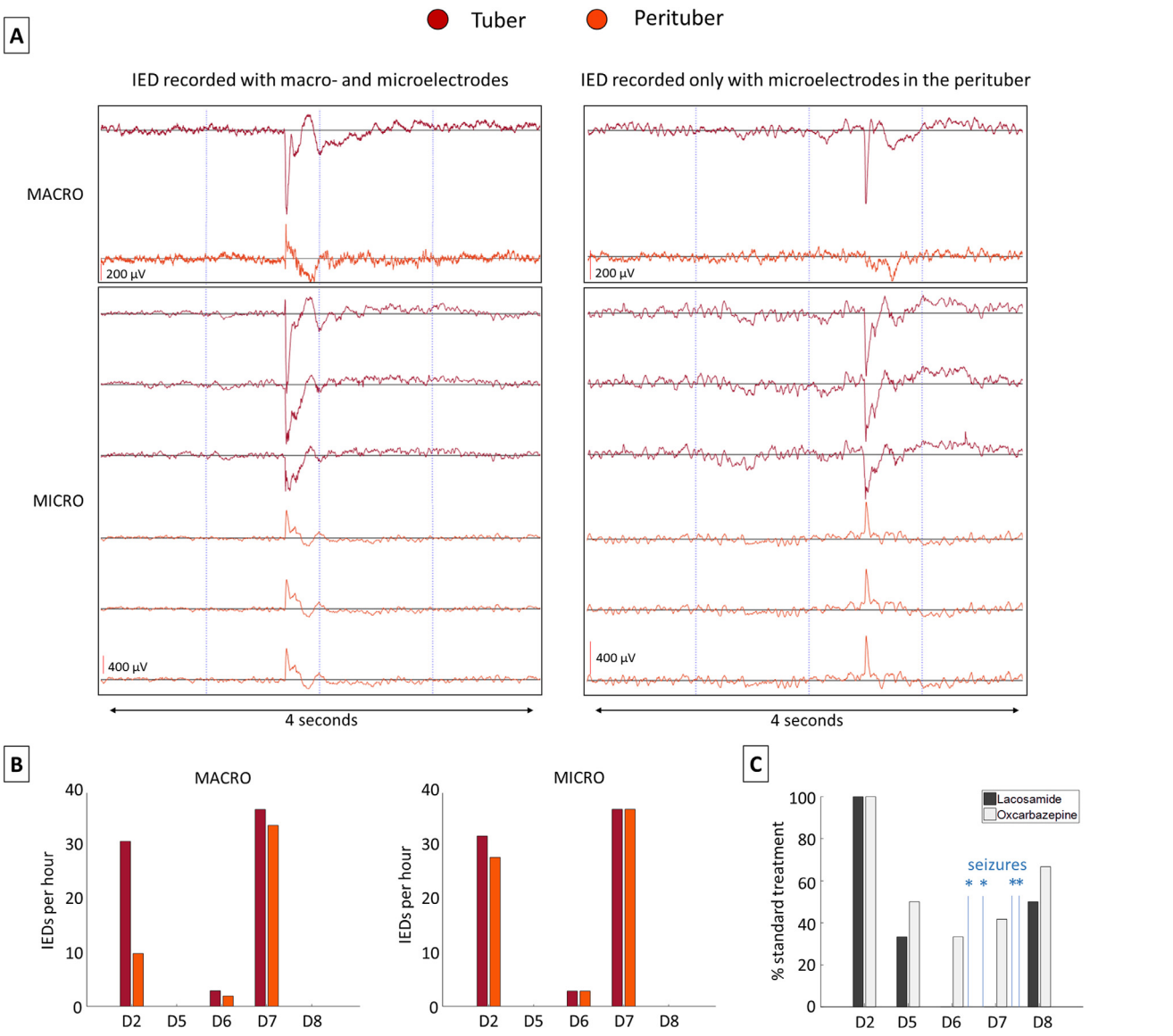

Fig. 3. (A) Example of an IED recorded simultaneously in the tuber (red) and perituberal tissue (yellow) with macro- and microelectrodes, and an example of another IED recorded in the perituberal tissue solely with microelectrodes. The signal of only one microwire per tetrode is shown. (B) Quantification of the IEDs during the 5 days of recordings in the tuber and perituberal tissue. (C) Change in the antiepileptic treatment associating lacosamide (300 mg per day) and oxcarbazepine (900 mg per day) during the same 5 days. Blue asterisks indicate the occurrence of spontaneous seizures. D n = recording during the n^{th} day after electrode implantation.

electrode, located adjacent to the perituber). IED occurrence varied throughout the SEEG. They clearly predominated on the second day and close to the spontaneous seizure occurrences after the antiepileptic treatment had been decreased (e.g. on Day 7, see Fig. 3B and C for details).

3.2. Neuronal activity

We focused our analyses on neuronal activity on Days 2 and 7, during which most of the IEDs were recorded (Fig. 3B). We recorded 84 neurons (21 in the tuber, 24 in the perituberal tissue, 8 in the amygdala, and 31 in the orbitofrontal cortex; see Supplementary Fig. S4 for details. The firing rates of 12 neurons (57%) in the tuber and four neurons (17%) in the perituberal tissue were modulated around the IEDs (chi2 test: $p = 0.01$; Fig. 4D). Action potential amplitudes and firing rates did not differ between modulated and nonmodulated neurons (Supplementary Figs. S5 and S6). In most cases, the firing of modulated neurons increased around the IEDs: 13 neurons (81%) had an increased firing rate during and/or after IEDs, whereas three (19%) had a decreased firing rate during and/or after IEDs (Fig. 4B and C). The firing rate of neurons recorded by tetrodes located in the amygdala and orbitofrontal cortex did not change during or around the IEDs recorded in the tuber and perituberal tissue.

Crosscorrelograms between all the pairs of neurons that were modulated during or outside the IEDs revealed three different functional interactions: synchronisation (simultaneous firing), inhibition, and delay (Fig. 4D and E). Outside the IEDs, tuberal neurons were highly synchronised, whereas one third of perituberal neurons tended to inhibit each other. Synchronisation between the tuber and perituberal tissue was only observed for one fifth of the pairs. During the IEDs, by contrast, we observed an overall decrease in synchronisation in both types of tissue, and perituberal neurons firing about 8 ms before tuberal neurons (one perituberal neuron fired 10 and 8 ms respectively before two different tuberal neurons. The other perituberal neuron fired 6 ms before another tuberal neuron).

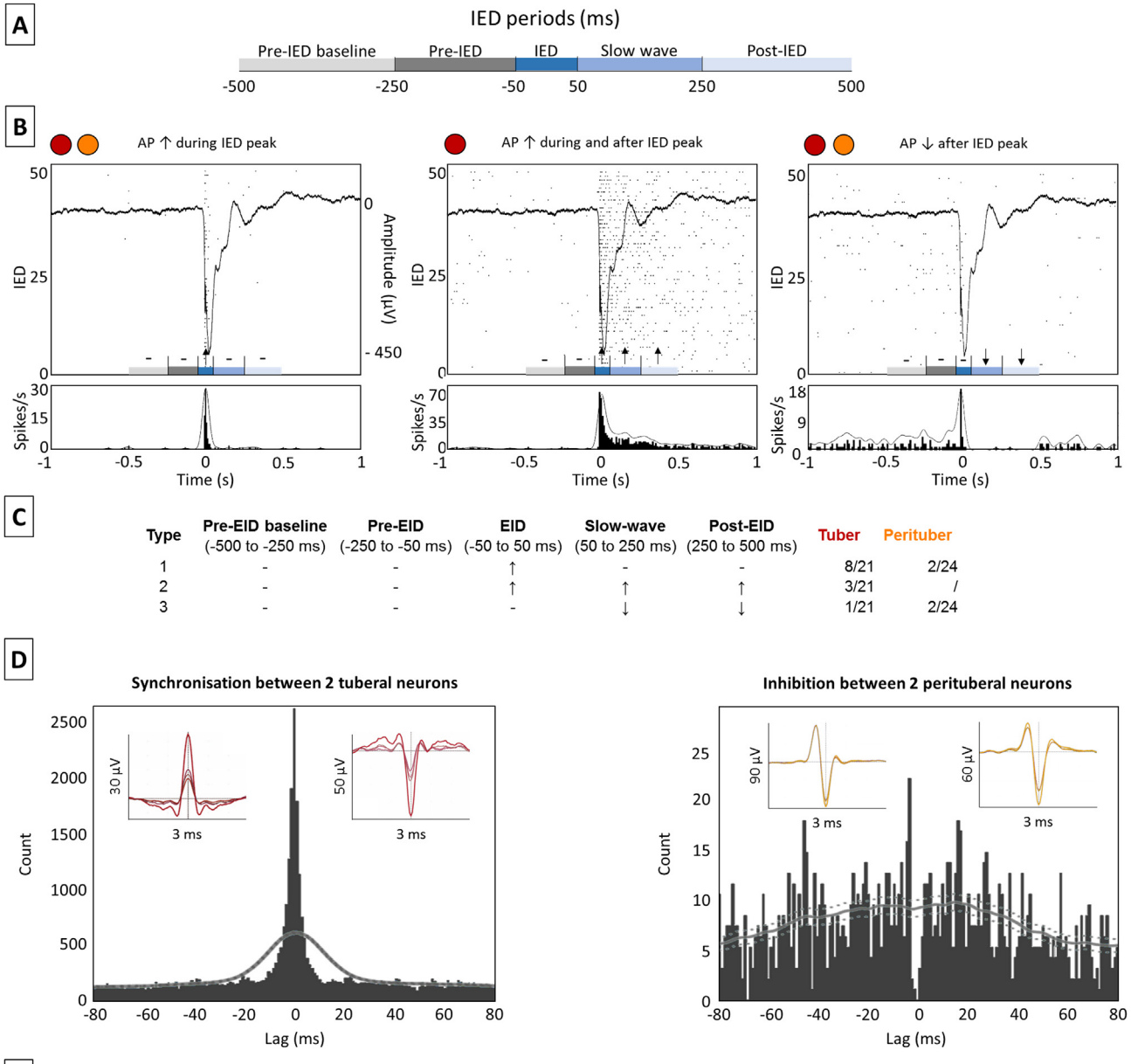

E

	Outside IEDs			During IEDs		
	% No FI	% FI	Type of FI	% No FI	% FI	Type of FI
Tuber-Tuber *(Ncomp = 31)*	39	61	synchronisation	62	38	synchronisation
Perituber-Perituber *(Ncomp = 6)*	67	33	Inhibition	100	0	/
Tuber-Perituber *(Ncomp = 28)*	80	20	synchronisation	90	10	delay (perituber few ms before tuber)

Fig. 4. (A) Timing of the five periods around each IED. We defined five distinct time periods around each IED peak (Time 0): pre-interictal discharge baseline period (−500 to −250 ms), pre-interictal discharge period (−250 to −50 ms), interictal discharge period (−50 to 50 ms), slow-wave period (50–250 ms), and post-interictal discharge period (250–500 ms). (B) Representative examples of the activity of three neurons recorded during 50 consecutives aligned IEDs in the tuber (red) and perituberal tissue (yellow). These were recorded on Day 7, when macro- and microelectrode signals were recorded for 90 min. The continuous line in the top part of the figure represents the mean of the 50 IEDs and the dots the raster plots of the neuronal activity. The bottom part of the figure represents the peristimulus time histograms. Time 0 and IED alignment were based on the IED peak. Three different patterns of activity could be distinguished: increased activity during the peak (left panel), increased activity both during and after the peak (middle panel), and decreased activity after the peak (right panel). Lack of significant change compared with the baseline period is indicated by dashes, and significant increases or decreases by up or down arrows ($p < 0.05$, Kruskal-Wallis one-way ANOVA with Dunn's post hoc test and Holm-Sidak correction). (C) Number of neurons of each type in the tuber and perituberal tissue. (D) Example of crosscorrelograms showing synchronisation and inhibition in the tuber and perituberal tissue. Dashed grey lines show the 99% confidence interval for the jittered spike trains. The averaged AP waveform for each neuron is shown above each crosscorrelogram. (E) Details of the functional interactions (FIs) found between all the modulated neuron pairs in the tuber and perituberal tissue. *Ncomp* = number of comparisons in each condition; AP: action potential.

3.3. FRs

We only recorded FRs with microelectrodes, and only in the insular tuber (op) (Fig. 5A). FRs were not recorded in the other tuber located in the medial superior frontal gyrus (macroelectrode PM). FRs had a mean duration of 14 ms (range: 9–20) and a mean frequency of 513 Hz (range: 431–562). However, their amplitudes varied (mean: 46 µV, range: 25–82). The five FRs with the highest amplitude were simultaneously recorded on two adjacent tetrodes, while the others were recorded on only one (Fig. 5B). FRs never

occurred during IEDs. FR occurrence varied throughout the SEEG: they clearly predominated on Day 7 (like the IEDs, when the spontaneous seizures occurred and when medication was reduced).

3.4. Seizures and clinical results

Semiology corresponded to the patient's usual seizures. The onset of three of the seizures was clearly identifiable and had exactly the same initial pattern (Fig. 6A): high-amplitude spike-and-wave activity simultaneously recorded in the insular tuber (medial contacts of macroelectrodes OP) and perituberal tissue (macroelectrodes H, medial contact of macroelectrode OF), followed by a low-voltage, high-frequency discharge. The fourth seizure began with a rhythmic slow-wave discharge in the tuber and perituberal tissue (macroelectrodes OF, OP, H), followed by the same pattern as the previous ones (Supplementary Fig. S2). The seizures did not involve the other tuber recorded by electrode PM. The mean normalised EI (calculated and averaged for the three seizures with a sharp and similar onset) was clearly higher in the tuber than in any other brain area explored by the macroelectrodes, including the perituberal tissue (Fig. 6B).

The insular tuber where the electrodes (OP-op) were located appeared hypometabolic, as the FDG-PET scan showed a clear asymmetry between right and left homologous regions (Fig. 1C). The microelectrodes in the perituberal tissue (h) were located in an area with normal or subnormal metabolism (Fig. 1C). Details of stimulation parameters and the induced effects are available in the Supplementary Material.

Based on the SEEG results, and before current analyses, the clinical decision was taken to carry out a cortectomy involving the right insular tuber. The limits of the cortectomy were determined according to MRI abnormalities, as well as the location of the electrodes. However, the patient has not yet undergone the operation, owing to a significant decrease in seizure frequency following the SEEG. Two and a half years after the SEEG, she was still seizure-free with an anti-epileptic medication.

4. Discussion

In the present study, we used new hybrid electrodes equipped with tetrodes to simultaneously analyse the interictal activity of tuberal and peritubeal tissues on the macro- and microscales, in order to better understand their respective roles in epilepsy.

IEDs were recorded in the same proportions and simultaneously in the tuber and perituberal tissue but had higher amplitude in the tuber. Furthermore, analysis of the EI suggested that the tuber was closer to the SOZ. Finally, FRs were recorded solely in the tuber. FRs clearly predominated on Day 7, when the antiepileptic treatment was as its lowest and spontaneous seizures were most numerous. As FRs are potential biomarkers of the SOZ, this further supports the notion that the tuber played a leading role in the generation of ictal EEG activity.

Interestingly, FRs were only detected with microelectrodes, in agreement with previous studies of other types of epilepsy, demonstrating that they are more easily recorded with microelectrodes (Zijlmans et al., 2017). An explanation is that FRs are produced by very small generators, which cannot be systematically recorded by macroelectrodes. Only in a minority of cases (22%), FRs were recorded simultaneously on two out of three tetrodes, and then only when their amplitudes were large (approximately >60 μV). In the other cases (78%) they were only detected by one of them. FRs were never simultaneously recorded on all three tetrodes, which supports the idea that they are generated within and confined to a small cortical region (Bragin et al., 1999; Demont-Guignard et al., 2012). It has been suggested that a small cluster of weakly synchronised hyperexcitable neurons (mainly

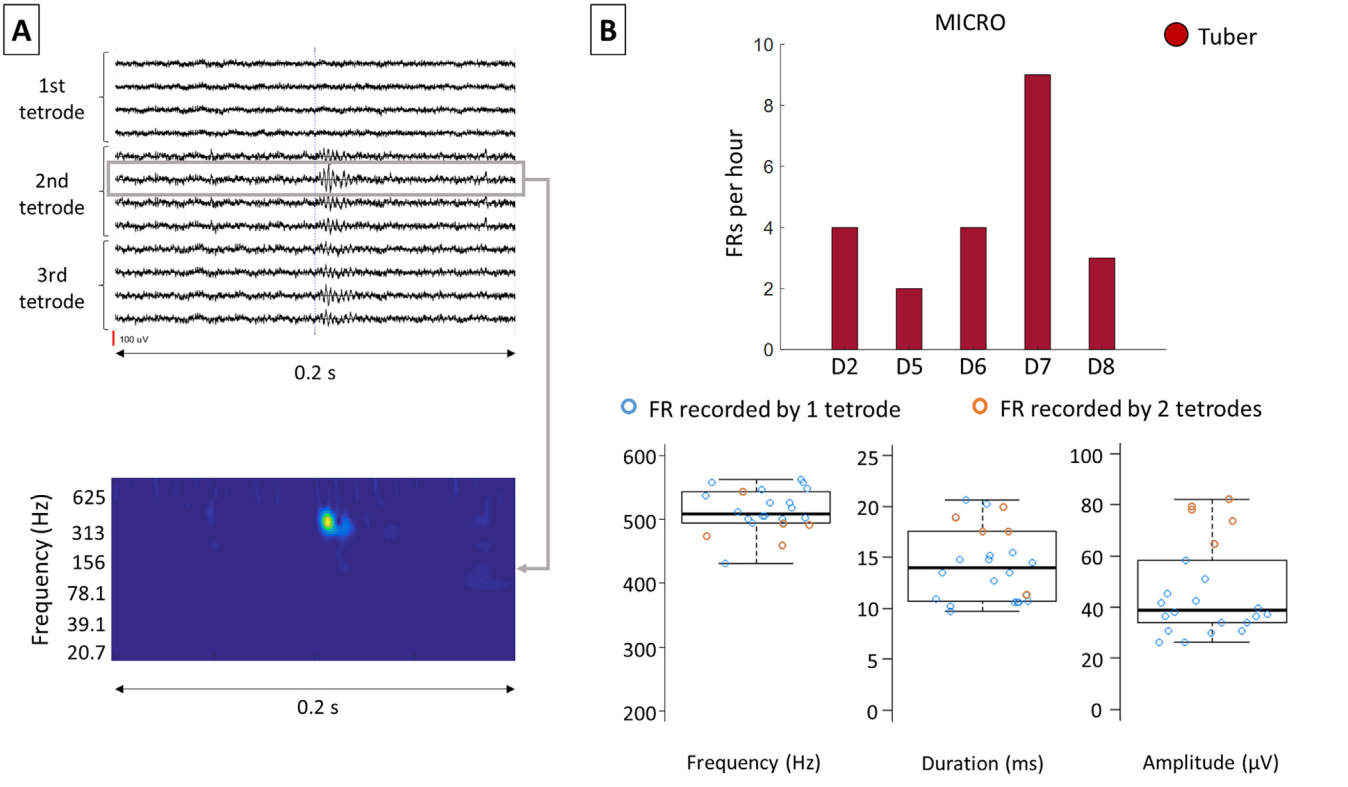

Fig. 5. (A) Example of a FR simultaneously recorded by two tetrodes on the same electrode. (B) FRs were only recorded in the tuber, and only with microelectrodes. Each circle corresponds to a FR. The orange circles correspond to the FRs that were recorded on two adjacent tetrodes, while the blue ones were all recorded on a single tetrode.

pyramidal cells) is responsible for generating FRs, whereas a larger number of hyperexcitable neurons generating a quasi-synchronous burst of action potentials is needed to generate IEDs (Demont-Guignard et al., 2012). Our tetrodes recorded a majority of tuberal (but not perituberal) neuron pairs with basal synchronisation, consistent with the tuber's propensity to generate FRs. Moreover, we showed that the dynamics of the relation between IEDs and FRs are not simple. We recorded FRs and IEDs on the same microelectrode contacts in the tuber, suggesting that the same epileptic tissue can generate both types of events, but we did not detect IEDs and FRs at the same time.

We recorded 21 neurons in the tuber and 24 in the perituberal tissue. For the first time, we found heterogeneous modulation of neuronal activity during IEDs in both structures, suggesting that they are both involved in IED generation. We found that 57% of tuberal neurons exhibited changes in firing rate during IEDs, compared with only 17% of perituberal neurons. The majority of the modulated neurons showed increased firing rates around the fast component of the IED. Recent years have seen a revision of the historical conception of a paroxysm of hypersynchronous excitatory activity during IEDs and seizures (Truccolo et al., 2011; Lambrecq et al., 2017). Our results are in line with these findings as they also reveal heterogeneous neuronal activity during IEDs. Studies of other lesions, such as cortical dysplasia and hippocampal sclerosis, have found that about 50% of neurons inside and outside the SOZ are correlated with surface IEDs, and approximately 40% increase their firing rates near the fast components of the IEDs (Wyler et al., 1982; Keller et al., 2010; Truccolo et al., 2011; Alvarado-Rojas et al., 2013). Our results thus appear convergent with these reports and suggest that they are general and independent of the brain area and its histological type. However, the higher proportion of changes in firing rates in the tuberal versus perituberal neurons around the IEDs strongly suggests that these changes vary according to the vicinity of the SOZ. We furthermore showed that neuronal spiking patterns can be heterogeneous in a very small region, as has already been demonstrated in other epileptic lesions during seizure onset and spread, or during IEDs (Wyler et al., 1982; Keller et al., 2010; Truccolo et al., 2011).

Previous conceptions of TSC epileptogenicity suggested a discontinuity between the tuber and perituber (Mohamed et al., 2012; Feliciano et al., 2013). Although we recorded similar numbers of neurons in the tuber and perituberal tissue, a smaller population of perituberal neurons than tuberal neurons was modulated around the IEDs. The fact that we observed neuronal

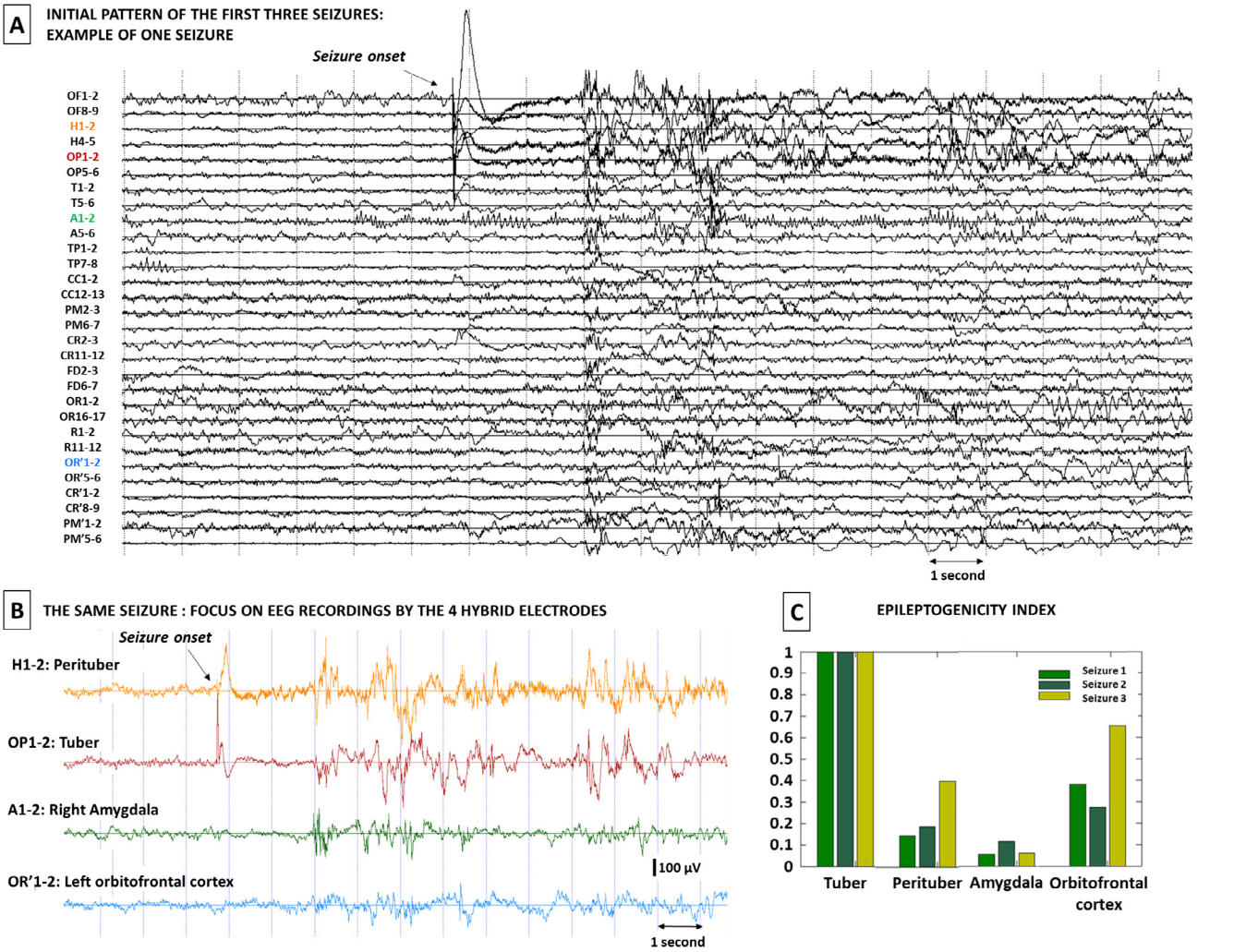

Fig. 6. (A) Example of a typical seizure recorded with the macroelectrodes. A view with all macroelectrodes (with a medial and lateral contact on each macroelectrode) is displayed. (B) The same seizure with a focus on the four hybrid electrodes (medial macrocontacts around the tetrodes). Visual analysis localised the seizure onset simultaneously in the tuber and perituberal tissue. This figure was obtained using the AnyWave toolbox (Colombet et al. 2015). (C) EI takes into account the delay in the appearance of this discharge with respect to the seizure onset. An EI between 0 and 1 reflects the secondary involvement of the brain structure in the seizure. The EI was computed for all seizures. The mean EI was higher in the tuber than in any other brain area.

activity in the perituber modulated during IEDs, rather than no relation at all, suggests that there is a *gradient of epileptogenicity* between these two structures. It has already been suggested that IEDs and seizures result from multiple synchronised clusters of pathological, interconnected neurons, and that the epileptogenic cortex may consist of a network of epileptogenic domains distributed among a majority of more normally functioning domains as small as 200 μm^2 (Bragin et al., 1999; Schevon et al., 2008; Truccolo et al., 2011). We can therefore hypothesize that these pathological clusters are widespread in both the tuber and peritubéral tissue in TSC lesions, but are more concentrated in the tuber. This hypothesis is congruent with recent studies showing a gradient of histological abnormalities between these two tissue types, from tuber centre to peritubéral tissue, favouring the notion that the brain lesions in TSC are more widespread than usually thought, and include sparse microtubers in an apparent healthy cortex (Peters et al., 2015; Sosunov et al., 2015).

Crosscorrelation analyses between each pair of modulated neurons highlighted a high level of synchronisation between tuberal neurons, which may be characteristic of neuronal interaction in brain areas that are isolated, or deafferented, from the rest of the cortex (Burns and Webb, 1979). Surprisingly, functional interactions between neurons during IEDs in both the tuber and perituber did not increase, but instead decreased slightly. This appears plausible with the idea that the pattern of neuronal activity was heterogeneous during IEDs. This suggests that the pattern of firing activity underlying IEDs might be more complex than previously thought and not limited to a hypersynchronous activity resulting from an imbalance between excitation and inhibition (Engel, 1996; De Curtis and Avanzini, 2001; Fisher et al., 2005), matching similar ideas about complex firing patterns during seizures (Keller et al., 2010). Although this high degree of synchronisation was not observed in peritubéral neuron pairs, 20% of tuberal and peritubéral neurons fired synchronously outside the IEDs and exhibited delayed firing activity during these IEDs, with peritubéral neurons firing around 8 ms before tuberal neurons. These results do no corroborate the hypothesis that an *isolated* tuber is the only structure involved in IED or seizure generation. Instead, it clearly points to interactions between the tuber and peritubéral tissue. This result is very interesting as it suggests that the gradient of epileptogenicity that was developed before is not unidirectional but probably more complex than this. This also questions the extent of the neurosurgery that has to be planned in TSC (Fallah et al., 2015).

Our study has several limitations. First, microelectrode recordings were limited to one hour per day and we did not record any seizure during that time. We are also aware that generalisation of our results is limited since they were obtained in only one patient and one tuber. In addition, the action potentials we recorded derived from only a few, indeterminate, elements of the neural circuitry such as pyramidal and inhibitory cells, a very small sample of the cortical neural circuitry that may involve thousands of neurons. This could lead to an overestimation of the complexity of the interactions (such as the 8 ms difference we report between the perituber and tuber) if too few cells of different types were recorded and require cautious interpretations of our results. However, this is the first time, to our knowledge, that microelectrode recordings have been performed in vivo in TSC, and have involved simultaneous recordings of tuberal and peritubéral tissues. Despite the previous limitations, such technically difficult recordings are a first and necessary step before getting large enough sampling of spike trains as this very specific implantation is rare and unlikely to occur often. It allowed us to perform analyses of the activity of neurons recorded in the tuber and perituber. Second, a surgical resection was not performed because of an unexpected decrease of seizure frequency after the SEEG in this patient. The exact histopathological type of tissue around our electrodes and the exact relations between electrode positions, giant cells and neurons cannot be analysed. However, delineation of tuber and perituber was rarely based on histological block of tissues in previous publications, and was done mostly on MRI variations, as in the current study (Ma et al., 2012; Kannan et al., 2016). It may also be argued that we cannot confirm our conclusions about the delineation of the SOZ given that it was not removed. However, we used a combination of markers of epileptogenicity already validated and reproduced across numerous studies, for instance fast ripples count and the epileptogenicity index, to support our reasoning.

5. Conclusion

Taken together, these results suggest that the tuber is critically involved in seizure onset, but that the interactions between the tuber and peritubéral tissue need to be taken into account. They support the idea of a gradient of epileptogenicity running from the tuber to the peritubéral tissue. Analysis of neuronal activity in both structures may gradually provide a better understanding of the mechanisms behind epileptogenicity in human TSC. There may be a variety of neuronal activities and interactions within and between these regions that needs to be taken into account in models of epilepsy in TSC. These results also question whether the neurosurgical resection needs to be extended to the perituber region (Fallah et al., 2015). As our results have been obtained in one patient and one tuber, they however need to be replicated in future studies.

Acknowledgments

This work received funding from the European Research Council, under the European Union's Seventh Framework Programme (FP/2007-2013) / ERC Grant Agreement no. 323711 (M4 project), the Fondation Française pour la Recherche sur l'Epilepsie (Prix Marion Clignet), the Fédération Française sur le Cerveau, and a call for technological and organisation innovation research projects (Toulouse University Hospital).

We would like to thank Dr Muriel Kany for the tuber and peritubéral tissue delimitation, and Felipe Rolando for his contribution to the identification of fast ripples.

Disclosure of conflicts of interest

ED is funded through a CIFRE industrial research agreement (no. 2015/1135) signed between Dixi Medical and the Centre de recherche Cerveau et cognition (CerCo). The remaining authors have no conflicts of interest.

Appendix A. Supplementary material

Supplementary data to this article can be found online at https://doi.org/10.1016/j.clinph.2018.12.013.

References

Alvarado-Rojas C, Lehongre K, Bagdasaryan J, Bragin A, Staba R, Engel J, et al. Single-unit activities during epileptic discharges in the human hippocampal formation. Front Comput Neurosci 2013;7:140.

Amarasingham A, Harrison MT, Hatsopoulos NG, Geman S. Conditional modeling and the jitter method of spike resampling. J Neurophysiol 2012;107:517–31.

Bartolomei F, Chauvel P, Wendling F. Epileptogenicity of brain structures in human temporal lobe epilepsy: a quantified study from intracerebral EEG. Brain 2008;131:1818–30.

Bartolomei F, Lagarde S, Wendling F, McGonigal A, Jirsa V, Guye M, et al. Defining epileptogenic networks: Contribution of SEEG and signal analysis. Epilepsia 2017;58:1131–47.

Bénar CG, Chauvière L, Bartolomei F, Wendling F. Pitfalls of high-pass filtering for detecting epileptic oscillations: a technical note on "false" ripples. Clin Neurophysiol 2010;121:301–10.
Bragin A, Engel J, Wilson CL, Fried I, Buzsáki G. High-frequency oscillations in human brain. Hippocampus 1999;9:137–42.
Burns BD, Webb AC. The correlation between discharge times of neighbouring neurons in isolated cerebral cortex. Proc Roy Soc Lond B Biol Sci 1979;203:347–60.
Chalifoux JR, Perry N, Katz JS, Wiggins GC, Roth J, Miles D, et al. The ability of high field strength 7-T magnetic resonance imaging to reveal previously uncharacterized brain lesions in patients with tuberous sclerosis complex. J Neurosurg Pediatr 2013;11:268–73.
Chu-Shore CJ, Major P, Camposano S, Muzykewicz D, Thiele EA. The natural history of epilepsy in tuberous sclerosis complex: Epilepsy in TSC. Epilepsia 2009;51:1236–41.
Colombet B, Woodman M, Badier JM, Bénar CG. AnyWave: A cross-platform and modular software for visualizing and processing electrophysiological signals. J Neurosci Methods 2015;242:118–26.
De Curtis M, Avanzini G. Interictal spikes in focal epileptogenesis. Prog Neurobiol 2001;63:541–67.
Demont-Guignard S, Benquet P, Gerber U, Biraben A, Martin B, Wendling F. Distinct hyperexcitability mechanisms underlie fast ripples and epileptic spikes. Ann Neurol 2012;71:342–52.
Engel J. Excitation and inhibition in epilepsy. Can J Neurol Sci 1996;23:167–74.
Fallah A, Rodgers SD, Weil AG, Vadera S, Mansouri A, Connolly MB, et al. Resective epilepsy surgery for tuberous sclerosis in children: determining predictors of seizure outcomes in a multicenter retrospective cohort study. Neurosurgery 2015;77:517–24.
Feliciano DM, Lin TV, Hartman NW, Bartley CM, Kubera C, Hsieh L, et al. A circuitry and biochemical basis for tuberous sclerosis symptoms: from epilepsy to neurocognitive deficits. Int J Dev Neurosci 2013;31:667–78.
Ferrari-Marinho T, Perucca P, Mok K, Olivier A, Hall J, Dubeau F, et al. Pathologic substrates of focal epilepsy influence the generation of high-frequency oscillations. Epilepsia 2015;56:592–8.
Fisher RS, van Emde Boas W, Blume W, Elger C, Genton P, Lee P, et al. Epileptic seizures and epilepsy: definitions proposed by the International League Againt Epilepsy (ILAE) and the International Bureau for Epilepsy (IBE). Epilepsia 2005;46:470–2.
Garcia S, Guarino D, Jaillet F, Jennings T, Pröpper R, Rautenberg PL, et al. Neo: an object model for handling electrophysiology data in multiple formats. Front Neuroinform 2014;8:10.
Gotman J, Gloor P. Automatic recognition and quantification of interictal epileptic activity in the human scalp EEG. Electroencephalogr Clin Neurophysiol 1976;41:513–29.
Grajkowska W, Kotulska K, Jurkiewicz E, Matyja E. Brain lesions in tuberous sclerosis complex. Rev Folia Neuropathol 2010;48:139–49.
Hill DN, Mehta SB, Kleinfeld D. Quality metrics to accompany spike sorting of extracellular signals. J Neurosci 2011;31:8699–705.
Jacobs J, Rohr A, Moeller F, Boor R, Kobayashi E, LeVan Meng P, et al. Evaluation of epileptogenic networks in children with tuberous sclerosis complex using EEG-fMRI. Epilepsia 2008;49:816–25.
Jansen FE, Van Huffelen AC, Algra A, Van Nieuwenhuizen O. Epilepsy surgery in tuberous sclerosis: a systematic review: epilepsy surgery in tuberous sclerosis. Epilepsia 2007;48:1477–84.
Kahane P, Landré E. The epileptogenic zone. Neurochirurgie 2008;54:265–71.
Kahane P, Landré E, Minotti L, Francione S, Ryvlin P. The Bancaud and Talairach view on the epileptogenic zone: a working hypothesis. Epileptic Disord 2006;8:16–26.
Kannan L, Vogrin S, Bailey C, Maixner W, Harvey AS. Centre of epileptogenic tubers generate and propagate seizures in tuberous sclerosis. Brain 2016;139:2653–67.
Keller CJ, Truccolo W, Gale JT, Eskandar E, Thesen T, Carlson C, et al. Heterogeneous neuronal firing patterns during interictal epileptiform discharges in the human cortex. Brain 2010;133:1668–81.
Lambrecq V, Lehongre K, Adam C, Frazzini V, Mathon B, Clemenceau S, et al. Single-unit activities during the transition to seizures in deep mesial structures: Seizures and Single-Unit Activities. Ann Neurol 2017;82:1022–8.
Ma TS, Elliott RE, Ruppe V, Devinsky O, Kuzniecky R, Weiner HL, et al. Electrocorticographic evidence of perituberal cortex epileptogenicity in tuberous sclerosis complex. J Neurosurg Pediatr 2012;10:376–82.
Madhavan D, Weiner HL, Carlson C, Devinsky O, Kuzniecky R. Local epileptogenic networks in tuberous sclerosis complex: A case review. Epilepsy Behav 2007;11:140–6.
Major P, Rakowski S, Simon MV, Cheng ML, Eskandar E, Baron J, et al. Are cortical tubers epileptogenic? Evidence from electrocorticography. Epilepsia 2009;50:147–54.
Marcotte L, Aronica E, Baybis M, Crino PB. Cytoarchitectural alterations are widespread in cerebral cortex in tuberous sclerosis complex. Acta Neuropathol 2012;123:685–93.
Mohamed AR, Bailey CA, Freeman JL, Maixner W, Jackson GD, Harvey AS. Intrinsic epileptogenicity of cortical tubers revealed by intracranial EEG monitoring. Neurology 2012;79:2249–57.
Munari C, Bancaud J. The role of stereo-electro-encephalography (SEEG) in the evaluation of partial epileptic patients. In: Porter RJ, Morselli PL, editors. The epilepsies. London: Butterworths; 1987. p. 267–76.
Narayanan NS, Laubach M. Methods for Studying Functional Interactions Among Neuronal Populations. In: Hyder F, editor. Dynamic Brain Imaging. Totowa, NJ: Humana Press; 2009. p. 135–65.
Okanishi T, Akiyama T, Tanaka S-I, Mayo E, Mitsutake A, Boelman C, et al. Interictal high frequency oscillations correlating with seizure outcome in patients with widespread epileptic networks in tuberous sclerosis complex. Epilepsia 2014;55:1602–10.
Peters JM, Prohl AK, Tomas-Fernandez XK, Taquet M, Scherrer B, Prabhu SP, et al. Tubers are neither static nor discrete Evidence from serial diffusion tensor imaging. Neurology 2015;85:1536–45.
Roehri N, Lina J-M, Mosher JC, Bartolomei F, Bénar C-G. Time-Frequency strategies for increasing high-frequency oscillation detectability in intracerebral EEG. IEEE Trans Biomed Eng 2016;63:2595–6.
Ruppe V, Dilsiz P, Reiss CS, Carlson C, Devinsky O, Zagzag D, et al. Developmental brain abnormalities in tuberous sclerosis complex: a comparative tissue analysis of cortical tubers and perituberal cortex. Epilepsia 2014;55:539–50.
Schevon CA, Ng SK, Cappell J, Goodman RR, McKhann G, Waziri A, et al. Microphysiology of epileptiform activity in human neocortex. J Clin Neurophysiol 2008;25:321–30.
Sosunov AA, McGovern RA, Mikell CB, Wu X, Coughlin DG, Crino PB, et al. Epileptogenic but MRI-normal perituberal tissue in Tuberous Sclerosis Complex contains tuber-specific abnormalities. Acta Neuropathol Commun 2015;3:17.
Sosunov AA, Wu X, Weiner HL, Mikell CB, Goodman RR, Crino PD, et al. Tuberous sclerosis: A primary pathology of astrocytes?: Astrocyte Pathology in Tuberous Sclerosis. Epilepsia 2008;49:53–62.
Truccolo W, Donoghue JA, Hochberg LR, Eskandar EN, Madsen JR, Anderson WS, et al. Single-neuron dynamics in human focal epilepsy. Nat Neurosci 2011;14:635–41.
Wyler AR, Ojemann GA, Ward AA. Neurons in human epileptic cortex: correlation between unit and EEG activity. Ann Neurol 1982;11:301–8.
Yger P, Spampinato GL, Esposito E, Lefebvre B, Deny S, Gardella C, et al. A spike sorting toolbox for up to thousands of electrodes validated with ground truth recordings in vitro and in vivo. ELife 2018;7 e34518.
Zijlmans M, Jiruska P, Zelmann R, Leijten FSS, Jefferys JGR, Gotman J. High-frequency oscillations as a new biomarker in epilepsy. Ann Neurol 2012;71:169–78.
Zijlmans M, Worrell GA, Dümpelmann M, Stieglitz T, Barborica A, Heers M, et al. How to record high-frequency oscillations in epilepsy: A practical guideline. Epilepsia 2017;58:1305–15.